Journal of Alloys and Compounds 537 (2012) 323–331

Contents lists available at SciVerse ScienceDirect

Journal of Alloys and Compounds

journal homepage: www.elsevier.com/locate/jalcom

An investigation of the Fe and Mo oxidation states in $Sr_2Fe_{2-x}Mo_xO_6$ ($0.25 \leqslant x \leqslant 1.0$) double perovskites by X-ray absorption spectroscopy

John R. Hayes, Andrew P. Grosvenor *

Department of Chemistry, University of Saskatchewan, Saskatoon, SK, Canada S7N 5C9

ARTICLE INFO

Article history:
Received 14 February 2012
Accepted 15 May 2012
Available online 24 May 2012

Keywords:
XANES
Order-disorder effects
Electronic structure
Data storage materials
Synchrotron radiation
Oxide materials

ABSTRACT

Sr_2FeMoO_6 double perovskite systems are widely studied because of their interesting and technologically relevant physical properties. Sr_2FeMoO_6 is just a single composition in the $Sr_2Fe_{2-x}Mo_xO_6$ solid-solution, and it is important to understand how the composition impacts the transition-metal valence states. Variations in the lattice parameters of these materials were studied using powder X-ray diffraction and it was found that a large change in the lattice constant occurs between $Sr_2Fe_{1.50}Mo_{0.50}O_6$ and $Sr_2Fe_{1.35}Mo_{0.65}O_6$ that likely coincides with a transition from a cubic to a tetragonal unit cell, in agreement with previous studies. Fe K- and Mo K-edge X-ray absorption near-edge spectra were also collected to investigate how the oxidation state and coordination environment change with composition. When the Mo content is low, Fe adopts a 3+ oxidation state and Mo adopts a 6+ oxidation state. As the Mo content is increased, the Fe and Mo cations are both *partially* reduced, resulting in a mixture of Fe^{3+} and Fe^{2+} and Mo^{5+} and Mo^{6+}. The reduction of the metal centers apparently drives the change in unit cell. The influence of preparation method on the oxidation states of Fe and Mo was also investigated by annealing the materials under vacuum. The results reported here show that the oxidation states of Fe and Mo are strongly impacted by both composition and preparation method, which may account for the wide variety of oxidation state and magnetic properties that have been reported previously.

1. Introduction

Double perovskite compounds, having the general formula $A_2BB'O_6$ (A = Alkaline-earth, B/B′ = transition metal), are well known to exhibit a variety of interesting and technologically relevant properties [1–4]. The basic double perovskite structure is an extension of the cubic perovskite structure (ABO_3) in which corner-sharing BO_6 and $B'O_6$ octahedra alternate, resulting in long-range ordering ($Fm\bar{3}m$; Fig. 1). When the size difference between the B and B′ cations is large, the structure may become tetragonally distorted, resulting in two distinct sites for the B and B′ ions (here, B represents the larger cation) [6,7]. This distortion results in the formation of one of two possible crystal lattices; one described by the I4/mmm space group and one described by the I4/m space group [8,9]. In the I4/mmm lattice, the B′ octahedra undergo compression along the c-axis while the B octahedra are elongated along the c-axis. In the I4/m unit cell, the B and B′ octahedra undergo opposing rotations, causing the octahedra to buckle, which results in expanded BO_6 octahedra and compressed $B'O_6$ octahedra [8,9]. The transition from the $Fm\bar{3}m$ structure to the I4/m structure is shown in Fig. 1. An example of a system that undergoes a transition from a cubic to a tetragonal lattice with variation in composition is the $Sr_2Fe_{2-x}Mo_xO_6$ double perovskite solid-solution. While X-ray diffraction studies have not conclusively shown whether $SrFeMoO_6$ adopts the I4/m or I4/mmm space group, the results of these distortions are similar, and the I4/m structure is assumed in this study [8,10,11]. This assumption is supported by a previous study which used group theory to suggest that I4/m symmetry must be adopted [12]. (This system is known to be oxygen-deficient, but it will be referred to here as $Sr_2Fe_{2-x}Mo_xO_6$ for simplicity [13,14]).

Sr_2FeMoO_6 has been shown to exhibit a variety of interesting magnetic properties [13,15–17]. For example, these materials are ferrimagnetic, with a Curie temperature reported to be between 410 and 450 K [9]. Here, ferrimagnetism arises from a double exchange mechanism, which results from the ferromagnetic alignment of Fe 3d electrons and the antiferromagnetic alignment of Mo 4d electrons [15,18,19]. This model assumes Fe adopts a 3+ oxidation state and Mo adopts a 5+ oxidation state, and the theoretical maximum saturation magnetization is 4 μ_B, though experimentally, the saturation magnetization has always been observed to be less [20–22]. This reduced experimental value has been linked to the amount of antisite disorder present, in which Fe occupies a Mo site (and vice versa), leading to antiferromagnetic coupling between adjacent Fe ions [14,23–27]. In addition to being ferrimagnetic, Sr_2FeMoO_6 is known to exhibit magnetoresistive

* Corresponding author. Tel.: +1 306 966 4660; fax: +1 306 966 4730.
E-mail address: andrew.grosvenor@usask.ca (A.P. Grosvenor).

0925-8388/$ - see front matter © 2012 Elsevier B.V. All rights reserved.
http://dx.doi.org/10.1016/j.jallcom.2012.05.056

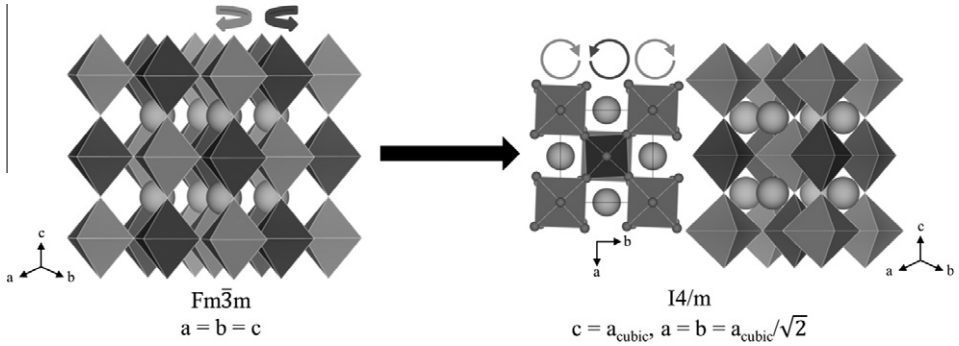

Fig. 1. The $Sr_2Fe_{2-x}Mo_xO_6$ compounds adopt one of two crystal structures. At low values of *x*, the undistorted, ordered double perovskite structure is adopted (space group $Fm\bar{3}m$, *left*,), consisting of alternating Fe (gray) and Mo (dark gray) octahedra with Sr atoms (light gray) occupying the interstitial sites. (The structure shown here represents a perfect Sr_2FeMoO_6 double perovskite.) As the value of *x* is increased, the Fe and Mo octahedra rotate (indicated by the circular arrows), resulting in FeO_6 octahedra that are stretched and MoO_6 octahedra that are compressed, and this results in a transition to a tetragonal unit cell (space group I4/m, *right*). The view along the *c*-axis (*center right*), shows the rotation of the octahedra (O atoms are shown as gray spheres). The relationship between the lattice constants from the two space groups is shown below each structure [5].

behavior, in which a decrease in the resistivity of the material is observed upon applying a magnetic field [23,24,28]. This behavior arises from the half-metallic character of Sr_2FeMoO_6, in which a spin-polarized band of Mo t_{2g}-O 2p-Fe e_g states crosses the Fermi level [16]. The magnetoresistive behavior has also been shown to be impacted by the presence of insulting grain-boundaries (when low magnetic fields are applied) and, because of this low-field magnetoresistance, Sr_2FeMoO_6 has been investigated for use in spintronic devices [23,29,30]. To better understand the origins of the aforementioned properties, and to better utilize these properties in technological applications, it is necessary to know what oxidation states are adopted by Fe and Mo in these compounds.

While there are a wide variety of studies on the valence states of Fe and Mo, no consensus has been reached [11,15,26,31–35]. Although no definitive values have been reported, the oxidation state of Fe is generally found to be between 2+ and 3+ while the oxidation state of Mo is found to be between 5+ and 6+ [15,21,18,31–35]. This disagreement probably arises from the complex nature of Sr_2FeMoO_6, with the material being sensitive to a wide variety of variables. For example, Sr_2FeMoO_6 is not a stoichiometric compound, but rather a member of the $Sr_2Fe_{2-x}Mo_xO_6$ ($0 \leqslant x \leqslant 2$) solid solution. As such, the system is sensitive to both the composition *and* synthetic conditions employed [14,36]. Despite this, no studies have directly investigated how the oxidation states of Fe and Mo vary in $Sr_2Fe_{2-x}Mo_xO_6$ materials with changing Mo content.

X-ray absorption near-edge spectroscopy (XANES) is a technique perfectly suited for such a study. In this technique, X-rays are used to excite core-level electrons to empty conduction states. Transition-metal (TM) K-edge XANES spectra, which result from an excitation of 1s core electrons, are especially sensitive to changes in the coordination environment and oxidation state of the metal center [37]. These spectra are typically divided into two regions; the pre-edge region consisting of excitations to TM $(n-1)$d states and the main edge region, which arises from excitations to TM np states. In general, the pre-edge region is weak because of the quadrapolar nature of these excitations and its lineshape is indicative of the coordination environment surrounding the TM center [38–42]. As the main-edge region results from dipolar transitions, the intensity of this feature is typically strong [37]. The absorption edge energy, defined as the inflection point of the absorption edge, is sensitive to changes in the oxidation state of the metal center [40,43,44]. In this study, Fe K- and Mo K-edge XANES spectra have been collected from a series of $Sr_2Fe_{2-x}Mo_xO_6$ compounds produced by the reaction of oxides under $H_{2(g)}$ in order to determine how the oxidation states of Fe and Mo depend on Mo content. These experiments have also provided information about how the oxygen deficiency (and coordination number) in these systems change with varying Mo content. Additionally, to better understand how preparation conditions might affect these oxidation states, Fe K- and Mo K-edge XANES spectra have been collected from samples that were annealed in a vacuum environment and compared to those from the originally prepared materials.

2. Experimental

2.1. Synthesis

A series of $Sr_2Fe_{2-x}Mo_xO_6$ (x = 0.25, 0.50, 0.65, 0.85, 1.0) compounds were synthesized via a common solid-state synthesis route [11,14,36]. Stoichiometric amounts of $SrCO_3$ (Alfa Aesar, 99%), MoO_3 (Acros Organics, >99%), and Fe_2O_3 (Alfa Aesar, 99.945%) were mixed and ground using an agate mortar and pestle. In materials with $x \geqslant 0.65$, the mixture was pressed into a pellet at 6 MPa and heated to 900 °C over 8 h under flowing 5% H_2 (balance N_2), held at 900 °C for 6–8 h (higher values of x required longer heating times), and cooled to room temperature over ~4.5 h. For materials with $x \leqslant 0.575$, it was found that pressing the precursor materials into a pellet resulted in a phase-impure material. In these cases, the loose powder was heated in air at 1100 °C for >12 h to decompose $SrCO_3$ to SrO. The powdered mixture was then heated to 900 °C over 8 h under flowing 5% H_2 (balance N_2), held at 900 °C for 3–4 h (higher values of x required longer heating times), and then cooled to room temperature over ~4.5 h. While many other studies have reported the use of higher temperatures (1000–1200 °C) to synthesize these materials, in this study, an acceptable level of phase purity could not be achieved using temperatures >900 °C when heated under 5% H_2 (balance N_2) [11,14,36]. In all cases, the gas flow was monitored using a mineral oil bubbler and the flow was kept at 1–2 bubbles/s. The flow rate was found to strongly impact the purity of the resultant product, as too high or too low a flow rate resulted in the formation of phase-impure materials, with Sr_2MoO_4 (too high a flow rate) and $SrMoO_4$ (too low a flow rate) comprising the principle impurity phases. The as-synthesized materials were also annealed under vacuum to study the impact of ordering on the oxidation states of the metal ions [42]. Aliquots of the as-synthesized samples were loaded into alumina crucibles and sealed in fused-silica tubes under rough vacuum and the samples were heated to 1050 °C from room temperature over ~7 h, held at this temperature for 12 h, and then slowly cooled to room temperature (~5 h).

Oxygen-deficient $SrFeO_{2.75}$-perovskite, $Sr_2Fe_2O_5$-brownmillerite, and FeO were also synthesized to act as standards. To synthesize the $SrFeO_{2.75}$ and $Sr_2Fe_2O_5$ samples, stoichiometric amounts of $SrCO_3$ (Alfa Aesar, 99%) and Fe_2O_3 (Alfa Aesar, 99.945%) were mixed, pelleted at 6 MPa, and heated in air at 1100 °C for 24 h. To control the O-stoichiometry, the samples were then reground, and subjected to separate heat treatments. The $SrFeO_{2.75}$ sample was heated at 1200 °C for 48 h, cooled to 600 °C, and held at this temperature for 24 h before being slowly cooled to room temperature. The $Sr_2Fe_2O_5$ sample was heated at 1200 °C for 48 h and quench-cooled in liquid nitrogen [45]. FeO was synthesized by mixing stoichiometric amounts of Fe metal powder (Alfa Aesar 99.5%) and Fe_2O_3 (Alfa Aesar, 99.945%) and pressing the resultant powder into a pellet at 6 MPa. The pellet was then heated at 900 °C for 12 h under flowing $N_{2(g)}$ [46,47]. Phase purity of all materials synthesized was determined using powder X-ray diffraction (XRD). Diffraction patterns were collected using a PANalytical Empyrean X-ray diffractometer equipped with a monochromatic Cu $K_{\alpha 1}$ (λ = 1.5406 Å) X-ray source. Lattice parameters were determined using the UnitCell software program by assuming a double perovskite cubic unit cell for all values of x in the chemical formula [48].

2.2. XANES

Fe K-edge and Mo K-edge spectra of the as-synthesized and annealed $Sr_2Fe_{2-x}Mo_xO_6$ samples were collected using the Pacific Northwest Consortium/X-ray Science Division Collaborative Access Team (PNC/XSD-CAT, Sector 20) bending magnet beamline (20BM) located at the Advanced Photon Source (APS), Argonne National Laboratory. A silicon (1 1 1) double crystal monochromator with harmonic rejection was used, which at 7000 eV has a resolution of 1 eV and a photon flux of $\sim 10^{11}$ photons/s [49]. Samples were finely ground and sandwiched between layers of Kapton tape and the number of layers of tape was varied to maximize absorption. Samples were mounted at a ~45° angle to the incident beam with transmission spectra being collected using N_2-filled ionization chambers while partial fluorescence yield spectra were collected using a Canberra 13-element Ge detector. The spectra were collected using an energy step of either 0.15 eV (Fe K-edge) or 0.30 eV (Mo K-edge) through the absorption edge. Spectra were calibrated using either an Fe reference foil (having a known Fe K-edge absorption-edge energy of 7112 eV) or a Mo reference foil (having a known Mo K-edge absorption energy of 20000 eV) [50]. The spectra from the reference foils were collected concurrently in transmission mode with the spectra from each oxide studied. All spectra collected were calibrated, normalized, and analyzed using the Athena software program [51]. As Sr_2FeMoO_6 materials have been shown to degrade into $SrMoO_4$ and other products over time, to eliminate the possibility of sample age significantly affecting the collected spectra, all spectra were collected within one month of sample preparation [52].

3. Results

3.1. Structure

To confirm phase purity, and to study how the structure of the $Sr_2Fe_{2-x}Mo_xO_6$ compounds change with varying Mo content, powder XRD patterns of the as-synthesized materials have been collected and are presented in Fig. 2. With the exception of Sr_2FeMoO_6, single phase $Sr_2Fe_{2-x}Mo_xO_6$ compounds were prepared. In the case of $SrFeMoO_6$, an 85–90% phase-pure material was synthesized, with small amounts (<6% each) of $SrMoO_3$, Sr_2MoO_4, and intermetallic $Fe_{1-x}Mo_x$ impurities being detected. (The exact composition of the intermetallic phase is not known [13].) The (1 0 1) reflection (denoted by an asterisk in Fig. 2), which corresponds to ordering of the Fe and Mo sites was only observed in the Sr_2FeMoO_6 compound, indicating a high degree of disorder in the other compounds synthesized [53]. It has been previously shown that the intensity ratio of the (1 0 1) reflection to the sum of the (2 0 0) and (1 1 2) reflections may be used as a measure of the amount of antisite disorder experienced by the Fe/Mo sites, with high values corresponding to less antisite-disorder [53]. For the as-synthesized $x = 1.0$ sample, the (1 0 1):((2 0 0)+(1 1 2)) ratio is 0.024, indicating that there is antisite disorder in this material. (In the compounds with $x < 1.0$, the ratio is zero, indicating that the amount of ordering of the transition metal sites in these systems is too low to be determined). Compared to previous studies, where the reaction temperature was higher (~1200 °C), this ratio was ~0.046, which suggests that the lower reaction temperature used in this study is not sufficient to achieve high levels of site ordering [11,53].

Upon annealing under vacuum, the XRD pattern (Fig. 3) shows that the ordering of Sr_2FeMoO_6 ($x = 1.0$) increases considerably compared to the as-synthesized version. The powder XRD patterns from the as-synthesized and vacuum annealed Sr_2FeMoO_6 samples (Fig. 3) show that in the as-synthesized materials, the (1 0 1):((2 0 0)+(1 1 2)) ratio is 0.024 while in the vacuum annealed sample, the ratio is 0.033. This observation implies that the material becomes more ordered upon annealing (i.e., the amount of antisite disorder is reduced) [53]. Additionally, the phase-purity of Sr_2FeMoO_6 increased dramatically with vacuum annealing, which was observed by the complete disappearance of peaks from the Sr_2MoO_4 and $Fe_{1-x}Mo_x$ phases in the powder XRD pattern (Fig. 3). In the other annealed $Sr_2Fe_{2-x}Mo_xO_6$ compounds ($x < 1.0$), no superstructural reflections were observed in the corresponding powder XRD pattern; however, the other reflections were observed to narrow considerably (not shown).

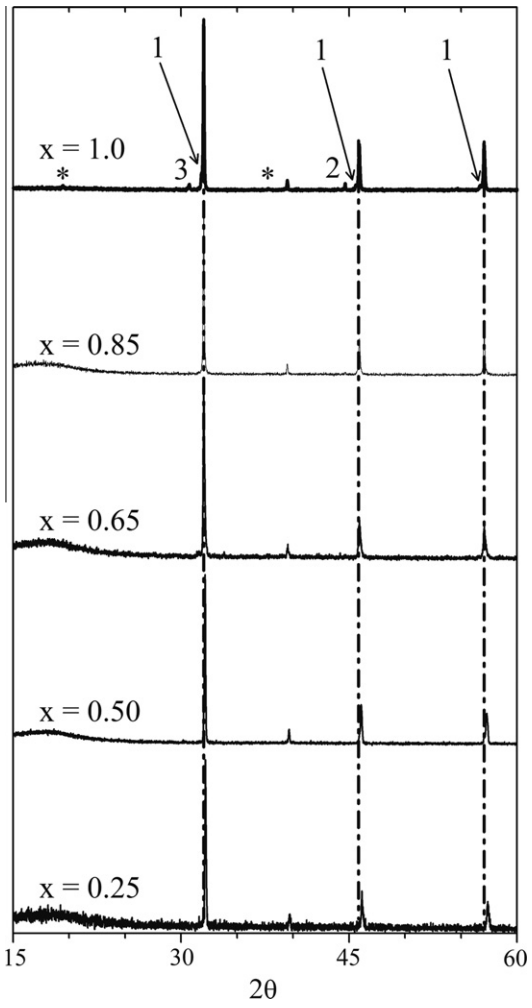

Fig. 2. Powder XRD patterns from as-synthesized $Sr_2Fe_{2-x}Mo_xO_6$ materials. Sr_2FeMoO_6 ($x = 1.0$) showed the following impurities: (1) $SrMoO_3$; (2) $Fe_{1-x}Mo_x$ intermetallic; and (3) Sr_2MoO_4. In addition, superstructural peaks from the tetragonal structure (denoted by asterisks) are observed in the Sr_2FeMoO_6 sample. All reflections were observed to shift to lower 2θ angles with increasing x. The broad feature found at ~18° in the patterns with $x < 1.0$ are from mineral oil, which was used to mount these samples.

The XRD patterns collected in this study were also used to calculate the lattice parameters of the $Sr_2Fe_{2-x}Mo_xO_6$ materials. The a lattice parameter was calculated assuming a cubic unit cell. The lattice constants are plotted as a function of Mo content in Fig. 4a, and show a sudden increase when $x \geqslant 0.65$. For all values of $x \geqslant 0.65$, the unit cell is observed to only increase slightly. This shift is also clearly observed in the powder XRD patterns (cf. Fig. 4b). The sudden and relatively large change in the lattice constant between $Sr_2Fe_{1.50}Mo_{0.50}O_6$ and $Sr_2Fe_{1.65}Mo_{0.35}O_6$ is indicative of a large change in the crystal lattice. In other structural studies of $Sr_2Fe_{2-x}Mo_xO_6$, this change has been shown to coincide with a transformation from a cubic to a tetragonal crystal structure. These studies performed Reitveld refinements on powder XRD data, and found the quality of the fit determined using a tetragonal model was higher than that determined using a cubic model when $x \geqslant 0.7$ [9,10,36]. In this study, upon annealing under vacuum, no significant changes in the lattice parameter were observed between the as-synthesized and annealed samples of a given composition.

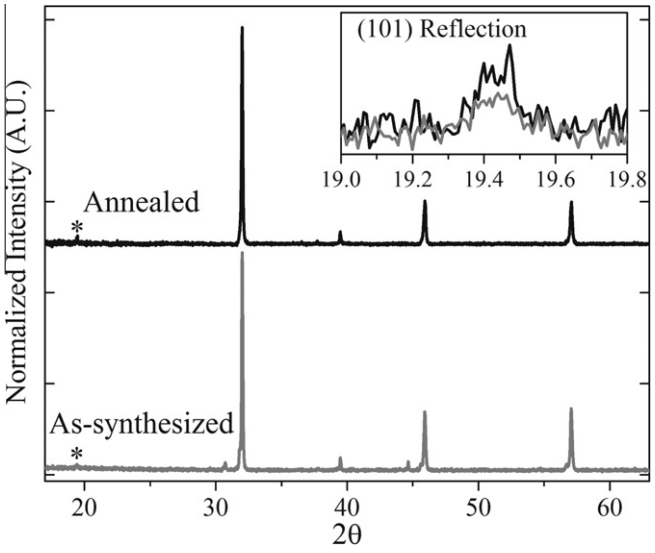

Fig. 3. The normalized powder XRD patterns from the as-synthesized (gray) Sr_2FeMoO_6 material and after being annealed under vacuum (black) are compared. Here, the patterns are offset along the y-axis for clarity. After annealing, the reflections at 30.6° and 44.7°, which are associated with impurity phases, were no longer observed. The (1 0 1) reflection (marked by an asterisk), is shown in the inset. The intensity of this reflection is greatly increased upon annealing in vacuum, indicating that a more ordered structure is present.

3.2. Fe K-edge XANES of the As-synthesized materials

Fe K-edge XANES spectra, which are presented in Fig. 5, were collected to determine the oxidation state of Fe in the $Sr_2Fe_{2-x}Mo_xO_6$ materials and to investigate the oxygen stoichiometry in these systems. Spectra from a series of standard compounds having known Fe oxidation states and coordination environments were also collected to aid in the interpretation of the $Sr_2Fe_{2-x}Mo_xO_6$ spectra, and are presented in Fig. 6. As is observed in Fig. 5a, there are four distinct features in the spectra from $Sr_2Fe_{2-x}Mo_xO_6$, which have been labeled as A, A′, B, and C. Features A and A′ make up the pre-edge region (see Fig. 5b), and are assigned to forbidden, quadrapolar, 1s → Fe 3d excitations [39]. By comparison with the Fe K-edge spectrum from FeO (Fig. 6), feature A is assigned to Fe^{2+} 1s → Fe 3d excitations, while comparison to the Fe K-edge spectra from $SrFeO_{2.75}$ and $Sr_2Fe_2O_5$ indicates that feature A′ is attributable to Fe^{3+} 1s → Fe 3d excitations. In $Sr_2Fe_{1.75}Mo_{0.25}O_6$, only feature A′ is observed, implying that only Fe^{3+} is observed in this compound. As the Mo content is increased to $x = 0.50$, feature A′ decreases in intensity and no other features are observed. As the coordination number (CN) of the Fe center decreases, and the local inversion symmetry is lost, 4p states overlap the 3d states, which adds a dipolar character to the pre-edge excitation. This increased dipolar character results in the observation of a more intense pre-edge peak (cf. spectra from $FePO_4{\cdot}xH_2O$ ($CN_{Fe} = 6$) and $SrFeO_{2.75}$ ($CN_{Fe} < 6$) in Fig. 6) [42,45]. (It should be noted that the increase in dipolar character is a result of changes in the local coordination environment only, and is not a result of long-range distortions of the crystal structure.) Comparing the spectra presented in Fig. 5 to those in Fig. 6 leads to the conclusion that the decrease in intensity of feature A′ observed in Fig. 5b as the Mo concentration is increased from $x = 0.25$ to 0.65 is a result of the system becoming less O deficient (i.e., the Fe CN increases). As the Mo content is further increased to $x \geqslant 0.65$, the intensity of feature A′ increases, as does the intensity of feature A, which implies that some Fe^{2+} is present. While feature A may contribute some intensity to feature A′ as the two features are not fully resolved, the fact that the intensities of both features increase

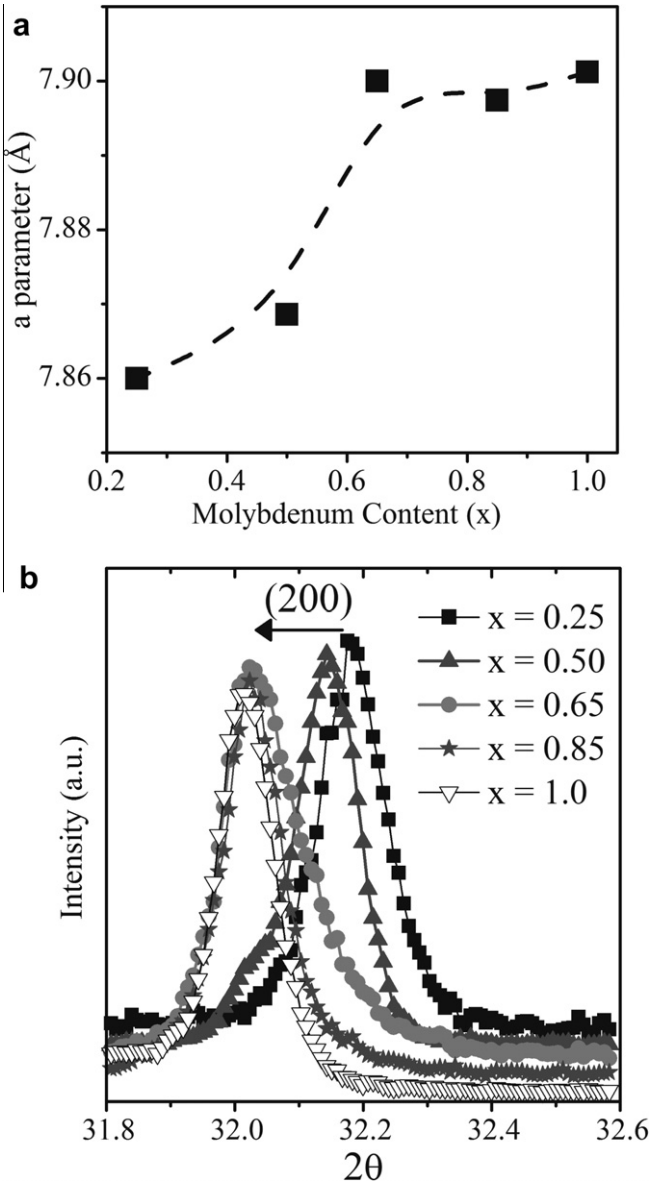

Fig. 4. (a) The lattice parameters calculated using a cubic unit cell for the $Sr_2Fe_{2-x}Mo_xO_6$ system as a function of Mo content (x) are shown. Between $x = 0.50$ and $x = 0.65$, a large increase is observed. The dashed line is included as a guide to the eye and the size of the symbols is representative of the uncertainty of the measurement. (b) The 2θ angle of the (220) reflection (indexing assumes a cubic structure) was found to shift to lower 2θ values as x increases. The large change in 2θ between $x = 0.50$ and 0.65 is reflective of the significant variation in the lattice shape.

simultaneously as x changes from 0.50 to 1.0 indicates that $Sr_2Fe_{2-x}Mo_xO_6$ becomes more O deficient as x increases from 0.65 to 1, as an increase in the concentration of Fe^{2+} would decrease the number of unoccupied Fe 3d states. Examination of Fig. 5b also indicates that the concentration of Fe^{2+} increases significantly as x is increased when $x \geqslant 0.65$.

To confirm the analysis of the changes in the pre-edge region, the main-edge can also be investigated. Features B and C comprise the main-edge, and arise from dipolar 1s → 4p excitations. By comparing the $Sr_2Fe_{2-x}Mo_xO_6$ spectra (Fig. 5) to the spectrum from FeO (Fig. 6), it is clear that feature B arises from the excitation of Fe^{2+} metal centers. As was the case for feature A in the pre-edge region, almost no change in intensity of feature B was observed as x was varied from 0.25 to 0.50; however, the intensity of feature B was

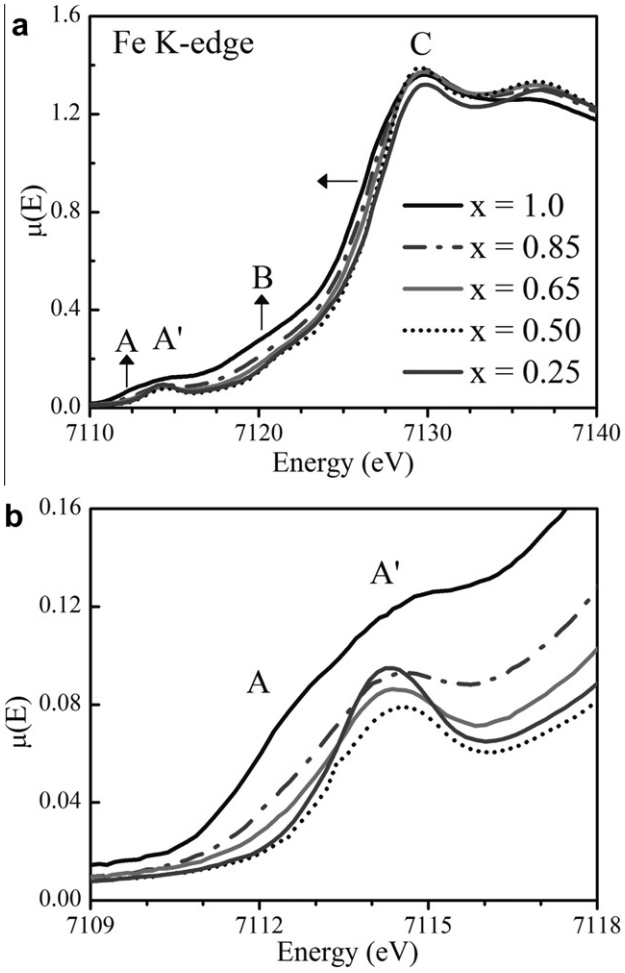

Fig. 5. (a) Fe K-edge spectra from the as-synthesized $Sr_2Fe_{2-x}Mo_xO_6$ materials are shown. Features A and A′ make up the pre-edge region and consist of transitions to Fe 3d states while features B and C are attributed to main-edge excitations resulting from Fe 1s → Fe 4p excitations. As the Mo content increases, features A and B increase in intensity and the absorption edge energy shifts to lower energy, indicating that the average Fe oxidation state is reduced (changes are shown by arrows). (b) The pre-edge region of the Fe K-edge spectra is shown. As the Mo content is increased, feature A significantly increases in intensity. The intensity of feature A′ is linked to the O deficiency of the materials and initially decreases as x is increased from $x = 0.25$ to 0.50. As x is increased to values greater than 0.50, the intensity of feature A is observed to increase.

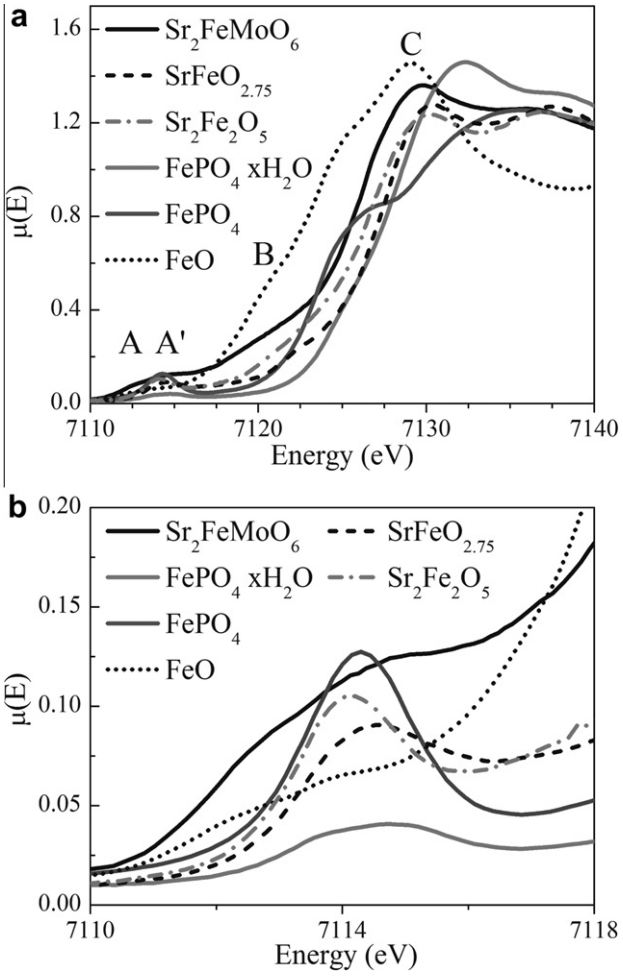

Fig. 6. (a) Fe K-edge spectra from a series of standards is presented along with the Fe K-edge spectrum from the as-synthesized Sr_2FeMoO_6 sample. (The spectra of $FePO_4$ and $FePO_4{\cdot}xH_2O$ are from reference [53].) (b) The pre-edge region of the Fe K-edge spectra is shown. Comparison of the spectra from Sr_2FeMoO_6 and FeO indicates that feature A is linked to the presence of Fe^{2+} while the link between the oxygen deficiency and the intensity of feature A′ is corroborated by comparison of the spectra from $SrFeO_{2.75}$ (CN < 6) and $Sr_2Fe_2O_5$ (average CN = 5).

found to vary significantly with increasing Mo content when $x \geqslant 0.65$. The presence of Fe^{2+} in these materials with varying x is further supported by the observed shifts in the main-edge energy of these spectra, which is defined as the inflection point of the main-edge (determined from the derivative spectrum by finding the peak maximum of the feature corresponding to the main-edge). The decrease in absorption energy with greater substitution of Fe for Mo ($\Delta E \approx 1.5$ eV), is ascribed to the presence of lower-energy valence Fe 4p-O 2p states, caused by increased ground-state screening of the Fe nuclear charge that results from a reduction of Fe^{3+} to Fe^{2+} [54].

The intensity of feature C initially increases between $Sr_2Fe_{1.75}Mo_{0.25}O_6$ and $Sr_2Fe_{1.50}Mo_{0.50}O_6$, but then remains relatively constant as the Mo content is further increased. This increase in intensity is likely linked to the O deficiency of the system. Given that there must be a fixed number of Fe 4p states, as the Fe 4p character of the pre-edge peak is reduced with increasing CN (i.e., decreased O deficiency; cf. Feature A′ Fig. 5b), the remaining Fe 4p states shift to higher energy and interact with the O 2p states (feature C), resulting in the observation of the increase in intensity of feature C in Fig. 5. Multiscattering resonances, which are part of the extended X-ray absorption fine structure (EXAFS), may also contribute to the intensity of feature C. The changes in the Fe K-edge XANES spectra as Mo content is increased may be summarized as follows: (1) for values of $x \leqslant 0.50$, Fe adopts a 3+ oxidation state; (2) when x is greater than 0.50, the average oxidation state of Fe decreases with increasing Mo content; (3) the O deficiency of the structure decreases as the Mo content increases when $x \leqslant 0.50$, but increases with increasing Mo content when $x > 0.50$; and (4) for no composition studied here was a fully oxygen stoichiometric compound synthesized.

3.3. Mo K-edge XANES of the As-synthesized materials

Mo K-edge spectra from the $Sr_2Fe_{2-x}Mo_xO_6$ compounds were collected to better understand how the Mo oxidation state changes with substitution, and are presented in Fig. 7a. In addition, to interpret changes in these Mo K-edge spectra, XANES spectra from several reference compounds were collected, and are presented in Fig. 7b. Two prominent features are observed in these spectra, and are labeled as D and E.

Feature D in Fig. 7 arises from forbidden transitions to Mo 4d states (much like in the Fe K-edge), and the intensity of this feature

appears to be related to the Mo content in $Sr_2Fe_{2-x}Mo_xO_6$ [55–58]. When $x = 0.25$ in $Sr_2Fe_{2-x}Mo_xO_6$, this feature is muted, while for higher values of x, the intensity of feature D increases. In all cases, the intensity of feature D is far less than that observed in the spectra from $SrMoO_4$ and MoO_3, in which Mo occupies a tetrahedral site or a highly distorted octahedral site, respectively (Fig. 7b). (In $SrMoO_4$, the highly distorted octahedra result in significant overlap between the Mo 4d and 5p states [59–61].) In the $Sr_2Fe_{2-x}Mo_xO_6$ compounds, the increase in the intensity of feature D with increasing Mo content suggests that, overall, the Mo coordination decreases with greater Mo content. However, this interpretation is tentative as it is difficult to separate changes in the intensity of feature D from shifts of the main absorption edge energy, given the poor energy resolution of Mo K-edge spectra (~4.5 eV when core–hole lifetime effects are considered) [58].

Feature E is attributed to the main-edge excitation, which arises from Mo 1s → Mo 5p excitations [58]. The main-edge energy is sensitive to changes in oxidation state and can be used to elucidate how the oxidation state of Mo in the $Sr_2Fe_{2-x}Mo_xO_6$ compounds changes with varying stoichiometry. Fig. 7c shows the derivative spectra from the $Sr_2Fe_{2-x}Mo_xO_6$ compounds along with that from the MoO_2 and $SrMoO_4$ reference compounds. When the Mo content is low ($x = 0.25$), the derivative maximum is at the same energy as that from the $SrMoO_4$ spectrum, indicating that Mo adopts an average oxidation state of 6+ in this material. As the Mo content increases in $Sr_2Fe_{2-x}Mo_xO_6$ to $x = 0.50$, the peak maximum of the derivative spectrum is observed to shift to lower energy, indicating a reduction in the Mo oxidation state (Fig. 7c). When the Mo content is further increased ($x = 0.65$), the derivative peak again shifts to lower energy, though it is still slightly higher than that of MoO_2 (Mo^{4+}). This observation suggests that Mo largely adopts a 5+ oxidation state when $x \geqslant 0.65$, though given the width of the MoO_2 derivative peak, it is possible that a minor quantity of Mo^{4+} is also present. (The width of the derivative peaks also shows that a small amount of Mo^{6+} is likely present when $x > 0.25$). Interestingly, as the Mo content is increased beyond $x = 0.65$, no further shifts in energy are observed.

3.4. Vacuum annealing

To understand how ordering of the Mo and Fe ions in $Sr_2Fe_{2-x}Mo_xO_6$ might impact the oxidation state and electronic environment of the metal centers, the as-synthesized compounds were annealed in an evacuated ampule and investigated by XANES. The Fe K- and Mo K-edge XANES spectra from these annealed compounds are compared to the corresponding spectra from the as-synthesized samples in Figs. 8 and 9, respectively. Large changes in the Fe K-edge spectra were observed between the as-synthesized and annealed $Sr_2Fe_{2-x}Mo_xO_6$ compounds when $x \geqslant 0.65$ (Fig. 8); however, no change was observed in the spectra from $Sr_2Fe_{1.75}Mo_{0.25}O_6$ and $Sr_2Fe_{1.50}Mo_{0.50}O_6$. For compounds where $x \geqslant 0.65$, features A, A′ and B decreased in intensity while the intensity of feature C was found to increase. These changes are consistent with the oxidation of Fe^{2+} in the $Sr_2Fe_{2-x}Mo_xO_6$ materials and an increase in the Fe CN. The source of oxygen is attributed to residual $O_{2(g)}$ left in the evacuated ampule. In previous studies on the synthesis of $SrMoO_3$, a compound that is related to the $Sr_2Fe_{2-x}Mo_xO_6$ compounds studied here, it was shown that oxygen partial pressures as low as 10^{-14} Torr could lead to the oxidation of $SrMoO_3$ [61–63]. As the ampules containing the annealed samples were only sealed under rough vacuum, the partial pressure of $O_{2(g)}$ present was much higher than 10^{-14} Torr. Oxidation of the Fe centers leads to an increase in the Fe CN, which was observed as a decrease in the intensity feature A′ owing to a decrease in mixing of the Fe 3d and 4p states. The decrease in intensity of feature A is also explained by the oxidation of Fe^{2+} to Fe^{3+}. Further,

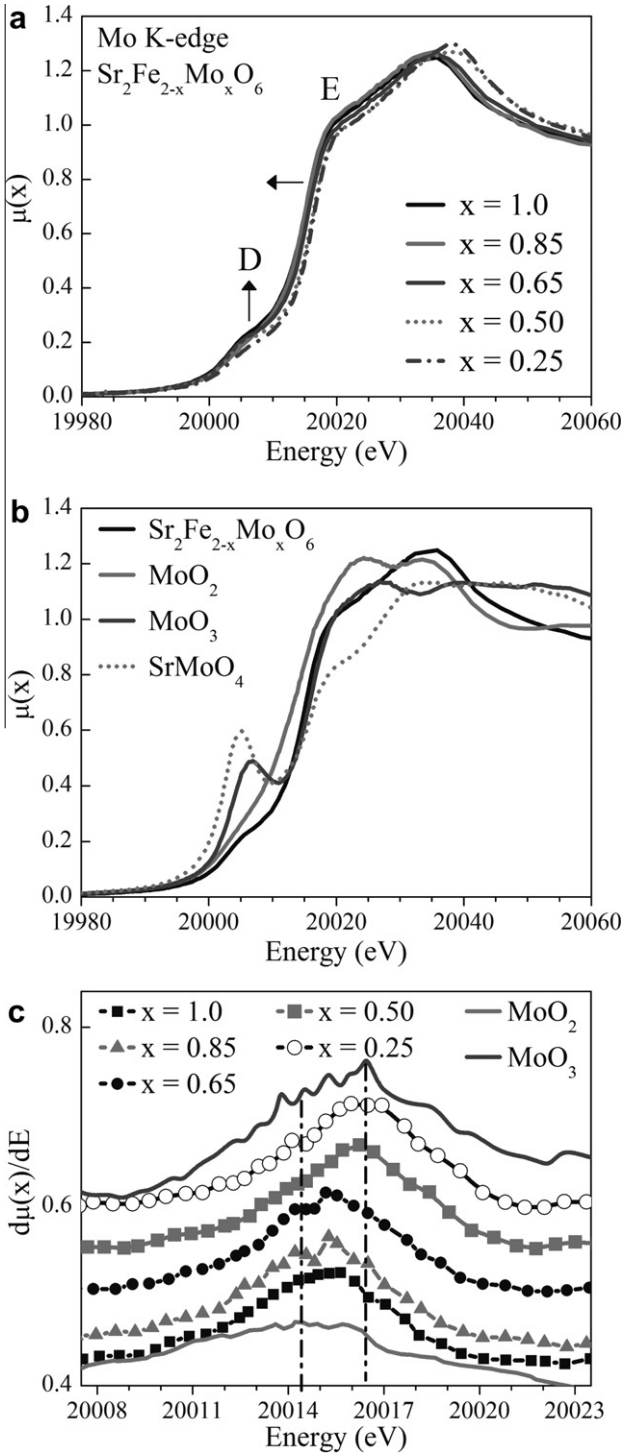

Fig. 7. (a) Mo K-edge spectra from the as-synthesized $Sr_2Fe_{2-x}Mo_xO_6$ materials. As the Mo content (x) increases, feature D increases in intensity, indicating a decrease in the Mo CN. Arrows are included to show how features change as x increases. (b) The Mo K-edge spectra from a series of standards, as well as the as-synthesized Sr_2FeMoO_6 sample, are plotted. (Mo adopts a 4+ oxidation state in MoO_2 and a 6+ oxidation state in MoO_3 and $SrMoO_4$.) (c) The derivative plot of the Mo K-edge spectra the $Sr_2Fe_{2-x}Mo_xO_6$ samples as well as the MoO_2 and MoO_3 standards is shown. For clarity, the MoO_2 derivative spectrum has been smoothed and the vertical dashed lines represent the peak energies of MoO_2 and MoO_3.

feature B (Section 3.2) was also observed to decrease in intensity, compared to the as-synthesized compounds because of the oxidation of Fe^{2+} to Fe^{3+}. The increase in intensity of Feature C was a result of the greater number of Fe 4p-O 2p states available for 1s

electrons to be excited to, which is indicative of an increased Fe CN [45]. Interestingly, the magnitude of the changes observed upon annealing increased with greater Mo content. The reason for this observation is simple: at higher Mo concentrations, the amount of Fe^{2+} present which can be oxidized is greater.

The Mo K-edge spectra of the annealed and synthesized samples (shown in Fig. 9) reveal that little to no change upon annealing. This observation does not indicate that no changes occur at the Mo sites. Instead, this result likely indicates that the magnitude of the changes is not detectable within the limits of the resolution of the Mo K-edge XANES spectra reported here.

4. Discussion

In this study, a series of $Sr_2Fe_{2-x}Mo_xO_6$ double pervoskites have been synthesized and studied by XANES to better understand the relationship between the concentration of Mo and the oxidation states of Fe and Mo, and the level of O deficiency in these materials. In $Sr_2Fe_{1.75}Mo_{0.25}O_6$, the Fe K-edge XANES spectrum (Fig. 5) indicates that Fe adopts a 3+ oxidation state while the Mo K-edge XANES spectrum (Fig. 7a) indicates that Mo adopts a 6+ oxidation state. Given the similarity of the effective ionic radii of Fe^{3+} and Mo^{6+} (0.645 and 0.59 Å, respectively), a near-random distribution of Mo^{6+} and Fe^{3+} would lead to an entropy stabilized system, which could be thought of as a solid-solution derivative of the cubic $SrFeO_{3-\delta}$ perovskite structure (here, δ indicates an unknown, but small amount of O deficiency) [7,8,64]. This suggestion is confirmed in this study by the lack of observation of the (101) reflection in the corresponding powder XRD patterns (Fig. 3). (While $SrFeO_{3-\delta}$ is reported to have a mix of Fe^{3+} and Fe^{4+} when δ is small, given the reducing conditions used to synthesize the $Sr_2Fe_{2-x}Mo_xO_6$ materials analyzed in this study, the formation of Fe^{4+} is not likely). In the case of $Sr_2Fe_{1.75}Mo_{0.25}O_6$, an oxygen deficient structure is required to achieve charge balance, as the maximum number of O atoms possible per formula unit is 5.4, assuming only Fe^{3+} and Mo^{6+} are present. Oxygen deficiency in this compound was confirmed in this study by the intense pre-edge feature in the Fe K-edge spectrum (Fig. 5). As the Mo content is increased to $Sr_2Fe_{1.50}Mo_{0.50}O_6$, the level of O deficiency is reduced, consistent with the replacement of Fe^{3+} by Mo^{6+} (as this leads to an overall increase of the average cationic charge). The increase in O content also explains the small increase of the lattice parameter (Fig. 4a) and the decrease in the pre-edge intensity in the corresponding Fe K-edge spectrum (Fig. 5b) as addition of large O^{2-} anions would expand the unit cell and increase the number of octahedrally coordinated Fe centers.

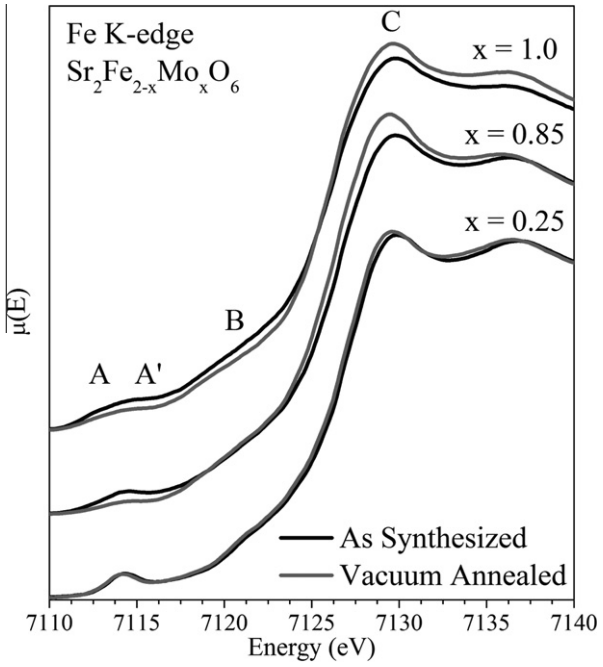

Fig. 8. The Fe K-edge spectra from several of the vacuum annealed $Sr_2Fe_{2-x}Mo_xO_6$ samples are presented along with the corresponding as-synthesized materials (spectra are offset for clarity). No change in the spectra were observed upon annealing when the Mo content is low ($x \leqslant 0.50$). When $x > 0.50$, the intensities of features A′ and B in the spectra from the vacuum annealed samples decrease compared to the as-synthesized samples, while the intensity of feature C increases. These observations indicate that the materials have been oxidized upon annealing and that the Fe CN increases.

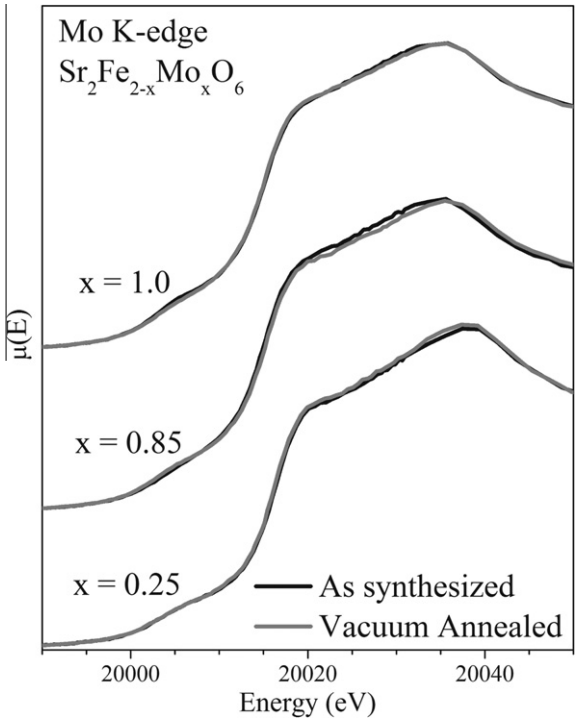

Fig. 9. The Mo K-edge spectra from several of the vacuum annealed $Sr_2Fe_{2-x}Mo_xO_6$ spectra are presented along with the corresponding as-synthesized materials (spectra are offset for clarity). Little to no change in the spectra was observed for all values of x.

As the Mo concentration was further increased to $x = 0.65$ ($Sr_2Fe_{1.35}Mo_{0.65}O_6$), the lattice parameter was calculated to be significantly larger than that of $Sr_2Fe_{1.50}Mo_{0.50}O_6$ (Fig. 4), and a large increase in the amount of Fe^{2+} and Mo^{5+} was observed in these materials, as shown by the changes in the Fe K-edge (Fig. 5; Section 3.2) and Mo K-edge spectra (Fig. 6a; Section 3.3). Here, it is proposed that between $x = 0.50$ and 0.65, a critical concentration of Mo is reached which allows for a reduction of both Fe and Mo without creating a destabilizing amount of O vacancies, as the oxidation state of Mo is always greater than that of Fe. The large shift in the lattice parameter (Fig. 4a) is attributed to a change in the unit cell shape from a cubic ($Fm\bar{3}m$) structure to a tetragonal (I4/m) structure (Fig. 1) [9,36]. As Fe^{3+} is reduced to Fe^{2+}, there is a dramatic increase in the effective ionic radius ($r_{Fe2+} = 0.780$ Å vs. $r_{Fe3+} = 0.645$ Å) while there is only a minor difference between the effective ionic radii of Mo^{6+} and Mo^{5+} ($r_{Mo5+} = 0.61$ Å vs. $r_{Mo6+} = 0.59$ Å) [64]. Thus, the tetragonal distortion of the lattice is the result of the steric distortions necessary to incorporate a significant amount of Fe^{2+}, which occupies the larger octahedral sites in this structure [9,10].

To determine how the ordering and O deficiency of the $Sr_2Fe_{2-x}Mo_xO_6$ materials is impacted by further heating, the

as-synthesized materials were annealed in a vacuum environment. Through examination of the Fe K-edge XANES spectra, oxidation of the Fe cations was observed to occur upon annealing the as-synthesized materials under vacuum. While oxidation of the Fe site results in a decrease of the average Fe radius and would be expected to decrease ordering based on the discussion above, analysis of the powder XRD patterns showed that the ordering of the Fe and Mo sites increased in Sr_2FeMoO_6 (Section 3.1; Fig. 4). This may be explained by the increased temperature used to anneal these samples (the samples were reduced at 900 °C (as synthesized) and annealed at 1050 °C), which apparently leads to increased ordering. Thus, these results serve to further confirm the dependence of the degree of ordering in $Sr_2Fe_{2-x}Mo_xO_6$ materials on temperature, as has been found in previous studies [11,30]. These results also suggest that the oxidation state of Fe found in Mo-rich $Sr_2Fe_{2-x}Mo_xO_6$ materials (those with $x \geqslant 0.65$) is highly sensitive to the atmosphere in which the materials are synthesized, consistent with studies of the related $SrMoO_3$ perovskite phase [62,63].

5. Conclusion

A series of $Sr_2Fe_{2-x}Mo_xO_6$ compounds were synthesized and studied by powder XRD and XANES to determine how the oxidation state of Fe and Mo depends on the Mo concentration. The powder X-ray diffraction patterns indicated that a large variation in the lattice parameter of these compounds occurred between the compounds with $x \leqslant 0.50$ and $x \geqslant 0.65$. This is in agreement with previous studies in which a transition from a cubic to tetragonal unit cell was reported [9,10,36]. Accompanying this change in structure is a *partial* reduction of the Fe oxidation state from Fe^{3+} to a mixture of Fe^{2+} and Fe^{3+} and a *partial* reduction of the Mo^{6+} oxidation state to a mixture of Mo^{5+} and Mo^{6+} (minor amounts of Mo^{4+} *may also* be present). Here, changes in the oxidation states of Fe and Mo have been spectroscopically shown to occur with changing Mo-content. Further, the results in this study indicate that the change in oxidation state of Fe from Fe^{3+} to $Fe^{2+/3+}$ is the driving factor in the transformation of the cubic lattice to a tetragonal lattice, and that the reduction of Fe is possible only after a *critical concentration* of Mo has been reached. The Fe K-edge XANES spectra also indicated that a significant amount of O vacancies exist in all of the materials studied. Upon annealing under a vacuum environment, $Fe^{2+/3+}$ was oxidized to Fe^{3+} and the oxygen deficiency of these compounds was significantly reduced. While O vacancies are already known to occur in these systems, using XANES, this study has shown that the amount of O deficiency is dependent on the amount of $O_{2(g)}$ present in the atmosphere in which these materials are reacted. The results reported here show that the composition strongly impacts the oxidation states of Fe and Mo in $Sr_2Fe_{2-x}Mo_xO_6$ materials, which are linked to structural changes within this system, and the dependence on both composition and preparation method likely accounts for the wide range of oxidation states and magnetic properties that have been reported previously.

Acknowledgements

The Natural Sciences and Engineering Research Council (NSERC) of Canada supported this work through a discovery Grant awarded to APG. JRH would also like to thank NSERC for financial support through the Canada Graduate Scholarship program. The University of Saskatchewan is thanked for funding provided to JRH. The Canadian Foundation for Innovation (CFI) is thanked for providing funds to purchase the PANalytical Empyrean powder X-ray diffractometer used in this work. The authors would also like to thank Prof. A. Mar (Department of Chemistry, University of Alberta) for providing access to the powder X-ray diffractometer located at the University of Alberta to perform preliminary measurements. Dr. Robert Gordon is thanked for his help in carrying out XANES measurements at 20BM (PNC/XSD-CAT, APS). The PNC/XSD facilities at the APS, and research at these facilities, are supported by the US Department of Energy - Basic Energy Sciences, a Major Resources Support Grant from NSERC, the University of Washington, Simon Fraser University and the APS. Use of the APS, an Office of Science User Facility operated for the U.S. Department of Energy (DOE) Office of Science by Argonne National Laboratory, was supported by the U.S. DOE under Contract No. DE-AC02-06CH11357.

References

[1] I.V. Solovyev, J. Magn. Magn. Mater. 268 (2004) 194–197.
[2] W. Prellier, V. Smolyaninova, A. Biswas, C. Galley, R.L. Greene, K. Ramesha, J. Gopalakrishnan, J. Phys.: Condens. Matter 12 (2000) 965–973.
[3] A. Millis, J. Nature 392 (1998) 147–150.
[4] S. Yousif, O.A. Yassin, J. Alloys Compd. 506 (2010) 456–460.
[5] K. Momma, F.J. Izumi, Appl. Cryst. 41 (2008) 653–658.
[6] P.M. Woodward, R.-D. Hoffman, A.W. Sleight, J. Mater. Res. 9 (1994) 2118–2127.
[7] F. Galasso, W. Darby, J. Phys. Chem. 66 (1962) 131–132.
[8] D. Serrate, J.M. De Teresa, M.R. Ibarra, J. Phys.: Condens. Matter 19 (2007) 023201.
[9] G.Y. Liu, G.H. Rao, X.M. Feng, H.F. Yang, Z.W. Ouyang, W.F. Liu, J.K. Liang, J. Alloys Compd. 353 (2003) 42–47.
[10] G.H. Rao, G.Y. Liu, X.M. Feng, Q. Zhang, J.K. Liang, Sci. Technol. Adv. Mater. 6 (2005) 750–754.
[11] B. Jurca, J. Berthon, N. Dragoe, P. Berthet, J. Alloys Compd. 474 (2009) 416–423.
[12] C.J. Howard, B.J. Kennedy, P.M. Woodard, Acta Crystallogr., Sect. B 59 (2003) 463–471.
[13] A. Sharma, A. Berenov, J. Rager, W. Branford, Y. Bugoslavsky, L.F. Cohen, J.L. MacManus-Driscoll, Appl. Phys. Lett. 83 (2003) 2384–2386.
[14] J. Rager, M. Zipperle, A. Sharma, J.L. MacManus-Driscoll, J. Am. Ceram. Soc. 87 (2004) 1330–1335.
[15] K. Kuepper, I. Balasz, H. Hesse, A. Winiarski, K.C. Prince, M. Matteucci, D. Wett, R. Szargan, E. Burzo, M. Neumann, Phys. Status Solidi 201 (2004) 3252–3256.
[16] K.-I. Kobayashi, T. Kimura, H. Sawada, K. Terakura, Y. Tokura, Nature 395 (1998) 677–680.
[17] M. Tovar, M.T. Causa, A. Butera, J. Navarro, B. Martínez, J. Fontcuberta, M.C.G. Passeggi, Phys. Rev. B 66 (2002) 024409.
[18] H. Jalili, N.F. Heinig, K.T. Leung, Phys. Rev B 79 (2009) 174427.
[19] A.W. Sleight, J.F. Weiher, J. Phys. Chem. Solids 33 (1972) 679–687.
[20] K.-I. Kobayashi, T. Okuda, Y. Tomioka, T. Kimura, Y. Tokura, J. Magn. Magn. Mater. 218 (2000) 17–24.
[21] S. Ray, A. Kumar, D.D. Sarma, R. Cimino, S. Turchini, S. Zennaro, N. Zema, Phys. Rev. Lett. 87 (2001) 097204.
[22] S. Ray, A. Kumar, S. Majumdar, E.V. Sampathkumaran, D.D. Sarma, J. Phys.: Condens. Matter 13 (2001) 607–616.
[23] D. Niebieskikwiat, F. Prado, A. Caneiro, R.D. Sánchez, Phys. Rev. B 70 (2004) 132412.
[24] A. Dinia, J. Vénaut, S. Colis, G. Pourroy, Catal. Today 89 (2004) 297–302.
[25] X.Z. Liao, A. Sharma, M. Wei, J.L. MacManus-Driscoll, W. Branford, L.F. Cohen, Y. Bugoslavsky, Y.T. Zhu, D.E. Peterson, Y.B. Jiang, H.F. Xu, J. Appl. Phys. 96 (2004) 7747–7749.
[26] J.-S. Kang, J.H. Kim, A. Sekiyama, S. Kasai, S. Suga, S.W. Han, K.H. Kim, T. Muro, Y. Saitoh, C. Hwang, C.G. Olson, B.J. Park, B.W. Lee, J.H. Shim, J.H. Park, B.I. Min, Phys. Rev. B 66 (2002) 113105.
[27] C. Meneghini, S. Ray, F. Liscio, F. Bardelli, S. Mobilio, D.D. Sarma, Phys. Rev. Lett. 103 (2009) 046403.
[28] C.A. López, M.-C. Viola, J.C. Pedregosa, J.A. Alonso, M.T. Fernández-Díaz, Eur. J. Inorg. Chem. 2010 (2010) 4110–4120.
[29] J.L. MacManus-Driscoll, A. Sharma, Y. Bugoslavsky, W. Branford, L.F. Cohen, M. Wei, Adv. Mater. 18 (2006) 900–904.
[30] D.D. Sarma, S. Ray, K. Tanaka, M. Kobayashi, A. Fujimori, P. Sanyal, H.R. Krishnamurthy, C. Dasgupta, Phys. Rev. Lett. 98 (2007) 157205.
[31] M.S. Moreno, J.E. Gayone, M. Abbate, A. Caneiro, D. Niebieskikwait, R.D. Sánchez, A. de Siervo, R. Landers, G. Zampieri, Solid State Commun. 120 (2001) 161–164.
[32] N. Menéndez, M. García-Hernández, D. Sánchez, J.D. Tornero, J.L. Martínez, J.A. Alonso, Chem. Mater. 16 (2004) 3565–3572.
[33] V. Kanchana, G. Vaitheeswaran, M. Alouani, A. Delin, Phys. Rev. B 75 (2007) 220404.
[34] J. Herrero-Martín, J. García, G. Subías, J. Blasco, M.C. Sánchez, J. Phys.: Condens. Matter 16 (2004) 6877–6890.
[35] M. Retuerto, F. Jiménez-Villacorta, M.J. Martínez-Lope, Y. Huttel, E. Roman, M.T. Fernández-Díaz, J.A. Alonso, Phys. Chem. Chem. Phys. 12 (2010) 13325–13616.
[36] T.-T. Fang, T.-F. Ko, J. Am. Ceram. Soc. 86 (2003) 1453–1455.
[37] L.A. Grunes, Phys. Rev. B 27 (1983) 2111–2131.
[38] G.A. Waychunas, M.J. Apted, G.E. Brown, Phys. Chem. Miner. 10 (1983) 1–9.

[39] F. de Groot, G. Vankó, P. Glatzel, J. Phys.: Condens. Matter 21 (2009) 104207.
[40] T.E. Westre, P. Kennepohl, J.G. DeWitt, B. Hedman, K.O. Hodgson, E.I. Solomon, J. Am. Chem. Soc. 119 (1997) 6297–6314.
[41] M.-A. Arrio, S. Rossano, Ch. Brouder, L. Galoisy, G. Calas, Europhys. Lett. 51 (2000) 454–460.
[42] J.-P. Reuff, L. Journel, P.-E. Petit, F. Farges, Phys. Rev. B 69 (2004) 235107.
[43] F. Farges, E. Chalmin, C. Vignaud, I. Pallot-Frossard, J. Susini, J. Bargar, G.E. Brown Jr., M. Menu, Phys. Scr. T115 (2005) 885–887.
[44] F. Farges, S. Rossano, Y. Lefrère, M. Wilke, G.E. Brown Jr., Phys. Scr. T115 (2005) 957–959.
[45] M.W. Gaultois, A.P. Grosvenor, J. Phys. Chem. C 114 (2010) 19822–19829.
[46] L. Chi, A.E.C. Green, R. Hammond, C.R. Wiebe, J.E. Greedan, J. Solid State Chem. 170 (2006) 165–175.
[47] E.R. Jette, F. Foote, J. Chem. Phys. 1 (1933) 29–36.
[48] T.J.B. Holland, S.A.T. Redfern, Mineral. Mag. 61 (1997) 65–77.
[49] S.M. Heald, D.L. Brewe, E.A. Stern, K.H. Kim, F.C. Brown, D.T. Jiang, E.D. Crozier, R.A. Gordon, J. Synchrotron Radiat. 6 (1999) 347–349.
[50] A. Thompson, D. Attwood, E. Gullikson, M. Howells, K.-J. Kim, J. Kirz, J. Kortright, I. Lindau, P. Pianetta, A. Robinson, J. Scofield, J. Underwood, D. Vaughan, G. Williams, H. Winick, X-ray Data Booklet, Lawrence Berkeley National Laboratory, Berkeley, 2009.
[51] B. Ravel, M. Newville, J. Synchrotron Radiat. 12 (2005) 537–541.
[52] K. Kuepper, M. Raekers, C. Taubitz, H. Hesse, M. Neumann, A.T. Young, C. Piamonteze, F. Bondino, K.C. Prince, J. Appl. Phys. 104 (2008) 036103.
[53] L1. Balcells, J. Navarro, M. Bibes, A. Roig, B. Martínez, J. Fontcuberta, Appl. Phys. Lett. 78 (2001) 781–783.
[54] J.A. Sigrist, M.W. Gaultois, A.P. Grosvenor, J. Phys. Chem. A 115 (2011) 1908–1912.
[55] K. Yokoi, N. Matsubayashi, T. Miyanaga, I. Watanabe, K. Murata, S. Ikeda, Chem. Lett. 16 (1987) 1453–1456.
[56] P.P. Samuel, S. Horn, A. Döring, K.G.V. Havelius, S. Reschke, S. Leimkühler, M. Haumann, C. Schulzke, Eur. J. Inorg. Chem. 2011 (2011) 4387–4399.
[57] H. Yan, R.A. Mayanovic, A.J. Anderson, P.R. Meredith, Nucl. Instrum. Methods Phys. Res., Sect. A 649 (2011) 207–209.
[58] F. Farges, R. Siewert, G.E. Brown Jr., A. Guesdon, G. Morin, Can. Mineral. 44 (2006) 731–753.
[59] C. Bernuy-Lopez, M. Allix, C.A. Bridges, J.B. Claridge, M. Rosseinsky, J. Chem. Mater. 19 (2007) 1035–1043.
[60] T. Leisegang, A.A. Levin, J. Walter, D.C. Meyer, Cryst. Res. Technol. 40 (2005) 95–105.
[61] A. Kuzmin, J. Purans, J. Phys.: Condens. Matter 12 (2000) 1959–1970.
[62] H.H. Wang, D.F. Cui, Y.L. Zhou, Z.H. Chen, F. Chen, T. Zhao, H.B. Lu, G.Z. Yang, M.C. Xu, Y.C. Lan, X.L. Chen, H.J. Qian, F.Q. Liu, J. Cryst. Growth 226 (2001) 261–266.
[63] I. Nagai, N. Shirakawa, S. Ikeda, R. Iwasaki, H. Nishimura, M. Kosaka, Appl. Phys. Lett. 87 (2005) 024105.
[64] R.D. Shannon, Acta Cryst. A32 (1976) 751–767.